JCI insight

PLA2G4A promotes right-sided colorectal cancer progression by inducing CD39+γδ Tregs polarization

Yang Zhan, … , Ti Zhang, Dalu Kong

JCI Insight. 2021. https://doi.org/10.1172/jci.insight.148028.

Research In-Press Preview Oncology

Graphical abstract

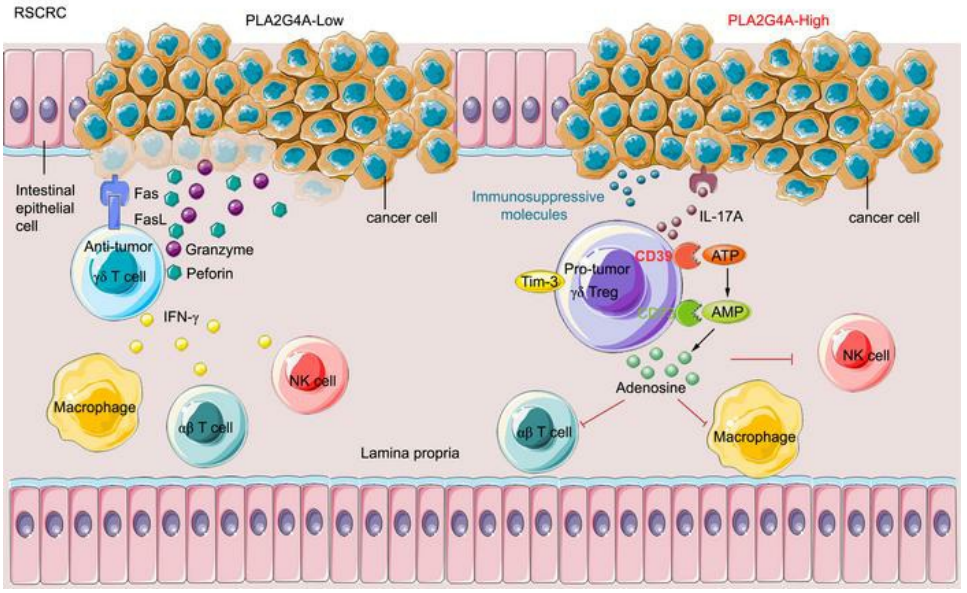

Find the latest version:

https://jci.me/148028/pdf

PLA2G4A promotes right-sided colorectal cancer progression by inducing CD39^{+}γδ Tregs polarization

Running title： Right-sided CRC induces CD39^{+}γδ Tregs

Yang Zhan[1], Lei Zheng[1], Jia Liu[1], Dongzhi Hu[1], Junfeng Wang[1], Kai Liu[1], Jiansheng Guo[1], Ti Zhang[1,2,*], Dalu Kong[1,*]

[1]Tianjin Medical University Cancer Institute and Hospital, National Clinical Research Center for Cancer, Tianjin's Clinical Research Center for Cancer, Key Laboratory of Cancer Prevention and Therapy, Tianjin, 300060, China

[2]Department of Hepatic Surgery, Fudan University Shanghai Cancer Center, Shanghai Medical College, Fudan University, Shanghai, 200032, PR China. (present address)

*Corresponding authors

Dalu Kong, Department of colorectal cancer, Tianjin Medical University Cancer Institute and Hospital; National Clinical Research Center for Cancer; Key Laboratory of Cancer Prevention and Therapy, Tianjin; Tianjin's Clinical Research Center for Cancer, Tianjin 300060, China. Phone: +86-022-23340123; Email: kongdalu@tjmuch.com;

Ti Zhang; Department of Hepatobiliary Surgery, Tianjin Medical University Cancer Institute and Hospital; Liver Cancer Center, Tianjin Medical University Cancer Institute and Hospital; National Clinical Research Center for Cancer; Key Laboratory of Cancer Prevention and Therapy, Tianjin; Tianjin's Clinical Research Center for Cancer, Tianjin 300060, China. Present address: Department of Hepatic Surgery, Fudan University Shanghai Cancer Center, Shanghai Medical College, Fudan University, Shanghai, 200032, PR China. Phone: +86-021-64175590； Email: zhangti@shca.org.cn

Conflict of interest: The authors have declared that no conflict of interest exists.

Abstract

γδ T cell is a promising candidate cell in tumor immunotherapy. However, γδ T cells polarized to $CD39^{+}$γδ Tregs upon colorectal cancer (CRC) induction and the underlying mechanism remains unclear. Here, we discovered that the frequency of $CD39^{+}$γδ Tregs, which positively correlated with poor prognosis, was significantly higher in right-sided CRC (RSCRC) than in the left-sided CRC (LSCRC). Interestingly, $CD39^{+}$γδ Tregs from RSCRC showed stronger immunosuppressive phenotype and function than LSCRC. Further, the quantitative mass spectrometry data showed that $CD39^{+}$γδ Tregs polarization was related to the abnormal activation of the PLA2G4A/AA metabolic pathway in RSCRC. Using an in vitro co-culture system and an orthotopic murine model of CRC, we proved that the overexpression of *Pla2g4a* in CT26 cells induced $CD39^{+}$γδ Tregs inhibiting the anti-tumor immune response. Finally, we found that the overall survival of the $PLA2G4A^{high}$ group was significantly shortened compared to $PLA2G4A^{low}$ RSCRC, while the survival of LSCRC was on the contrary. Collectively, RSCRC with abnormal PLA2G4A expression educates γδ T cells into $CD39^{+}$γδ Tregs to promote tumor progression and metastasis. Our work highlights the interaction between cancer cells and immune cells by distinguishing the primary tumor site and deepens the understanding of tumor microenvironment and immunosuppression.

Keywords: CD39; Regulatory γδ T cells; colorectal cancer; Immunosuppression

Introduction

Colorectal cancer (CRC) ranks the third among the most common cancers and has become the second leading cause of cancer death in the world, seriously threatening people's lives and health (1). The 5-year relative survival rate was only 11.7% for patients with distant metastasis (2). Although immunotherapy, especially PD-1/PD-L1 blockades, has achieved great success in advanced melanoma, non-small cell lung cancer, and Hodgkin's lymphoma，it was only effective in 4% metastasis CRC (mCRC) patients (3). Tumor cells establish an immunosuppressive microenvironment to evade immune surveillance, which becomes the major obstacle in immunotherapy, especially in solid tumors, such as CRC (4). Therefore, a better understanding of the immunosuppressive microenvironment in CRC is critical.

Prognostic stratification based on molecular classification is expected to make individualized treatment for patients. A large number of studies have confirmed that there are significant differences in embryonic origin, anatomical supply, clinical manifestations, and molecular genetics of the left-sided (LSCRC) and right-sided colorectal cancer (RSCRC) (5-7). The left hemicolon originates from the posterior intestine of the embryo and is supplied by the submesenteric artery. The right hemicolon originates from the central intestine and is supplied by the superior mesenteric artery. LSCRC is common in young male patients, while RSCRC is common in old female patients. The primary tumor site is also an independent predictor of anti-EGFR, anti-VEGF treatment, and prognosis of stage IV colorectal cancer (8-10). Venook's CALGB/SWOG 80405 clinical data were published in ASCO in 2016 and showed that the survival of patients with RSCRC is significantly shortened compared to III-IV-stage LSCRC (11). The latest research confirmed that the primary tumor location significantly impacts CRC prognosis (12). In 2017, the national comprehensive cancer network (NCCN) guidelines recommended for the first time that the primary tumor site should be included in the reference basis for the selection of targeted drugs in the first-line treatment of advanced CRC (13). In 2019, NCCN issued guidelines for diagnosing and treating colorectal cancer, which once again put forward the difference of medication for LSCRC/RSCRC (cetuximab is no longer recommended for preoperative conversion therapy for advanced RSCRC). However, the current research has not explored the molecular mechanism of the difference between the two

and could not break through the existing treatment. Therefore, it is urgent to explore the molecular mechanism of LSCRC/RSCRC progression difference.

Tregs are vital immunosuppressive cells that contribute to suppressing immune responses, mediating immune tolerance, and facilitating tumorigenesis and metastasis. Although traditional αβ TCR-presenting Tregs, such as $CD4^+$ or $CD8^+$Tregs, have been extensively studied [9], much less is known about intra-tumor γδ Tregs. Recently, a novel $CD39^+$γδ Treg in human CRC has been identified (14). $CD39^+$γδ Tregs are the predominant regulatory T cells in CRC and mediated direct and robust immunosuppressive effect on $CD3^+$ T cells via the adenosine pathway but independent of TGF-β or IL-10 (14). However, the roles and underlying mechanism of $CD39^+$γδ Tregs in LSCRC/ RSCRC's immunosuppressive microenvironment remain unclear.

In this study, we revealed a higher accumulation of tumor-infiltrating $CD39^+$γδ Tregs in RSCRC than paired normal tissue and LSCRC, along with increased production of IL-17A and adenosine, consequently enhanced the immunosuppressive function. Furthermore, PLA2G4A/Arachidonic acid metabolic pathway was abnormally activated in RSCRC, which induced $CD39^+$γδ Tregs polarization and indicated a poor prognosis.

Results

The frequency of tumor-infiltrating CD39$^+$γδ Tregs was significantly increased in RSCRC compared with LSCRC

The CD39-adenosine pathway is important in regulating the immune system and tumor immunosuppressive microenvironment (15-17). A previous study has identified CD39$^+$γδ T cells as a subset of Tregs with strong immunosuppressive functions, and they correlated positively with malignant clinicopathological features in human CRC (14). However, the distribution and functional changes in different tumor microenvironments remain unclear. In the present study, we found that the frequencies of CD39$^+$γδ Tregs were changed between RSCRC and LSCRC. Compare to the paired normal control (14.72% ± 13.21%), the frequency of tumor-infiltrating CD39$^+$γδ Tregs was significantly increased in RSCRC (28.87% ± 14.94%), while it was decreased in LSCRC (11.08% ± 7.83%, P<0.001, n=35; Figure1 A and B). In addition, the infiltration of CD4$^+$CD39$^+$T cells tended to decrease (normal vs. tumor = 14.43% ± 12.67% vs. 7.01% ± 8.73%, P=0.22; Figure1 A and C) and the frequency of CD8$^+$CD39$^+$T cells (normal vs. tumor = 8.60% ± 4.58% vs. 12.02% ± 12.92%, p=0.67; Figure1 A and D) tended to increase in RSCRC. Notably, these tumor-infiltrating γδ T cells (γδ-TILs) were dominantly Vδ1 subset, indicating that they are derived from intestinal tissue resident γδ T cells (Supplementary Figure 1).

Differentiation phenotype of CD39$^+$γδ Tregs in RSCRC/LSCRC

The anti-tumor function of γδ T cells is mainly based on IFN-γ production (18), while the pro-tumor function is linked to IL-17 production (19-21). Thus, we measured the productions of these two cytokines in tumor-infiltrating CD39$^+$γδ Tregs. The flow cytometry results showed that IL-17A-producing CD39$^+$γδ Tregs in RSCRC was dramatically increased compared with the paired normal tissues (60.46% ± 5.82% vs. 31.44% ± 2.74%, P=0.004), while significantly down-regulation of IL17A was detected in CD39$^+$γδ Tregs in LSCRC (6.85% ± 1.54%; Figure 2A and B). Compared to normal tissues, the level of IFN-γ-producing CD39$^+$γδ Tregs in RSCRC was decreased (8.36% ± 2.29% vs. 1.35% ± 0.86%, P=0.043), and

which was no change in LSCRC (Figure 2A and C). These data indicated the stronger pro-tumor function of CD39$^+$γδ Tregs in RSCRC than their left-sided counterpart, which may relate to the worse prognosis of patients with RSCRC.

Next, we detected the expression of immune checkpoint molecules (22, 23) on CD39$^+$γδ Tregs in different primary tumor sites by flow cytometry. Interestingly, the expression of PD-1 was significantly increased on CD39$^+$γδ Tregs in LSCRC compared to that in paired normal tissues (17.06%$\pm$2.87% vs. 4.19%$\pm$1.06%, P=0.033), while a substantial increase of Tim-3 was found on CD39$^+$γδ Tregs in RSCRC (40.76%$\pm$12.44%, Figure 2D and E). These data showed that the differentiation phenotype of CD39$^+$γδ Tregs in RSCRC/LSCRC, thus the target of cancer immunotherapy for patients with RSCRC/LSCRC, should be distinguished.

CD39$^+$γδ Tregs in RSCRC showed enhanced immunoregulatory function and positively correlated with malignant clinicopathological features

It has been proved that the inhibitory effect of CD39$^+$γδ Tregs on effector T cells is achieved by direct secretion of adenosine (14). Therefore, we next sorted tumor-infiltrating CD39$^+$γδ Tregs from patients with double primary colorectal cancer (RSCRC and LSCRC) and then detected adenosine in the supernatant by HPLC after cultured for 5 days. We found that the adenosine level secreted by CD39$^+$γδ Tregs in RSCRC was significantly higher than that in the left counterpart (P<0.01, n=5). Compared to paired normal tissues, CD39$^+$γδ Tregs in RSCRC secreted much more adenosine in the supernatant (Figure 3A). In order to determine the direct suppression of CD39$^+$γδ Tregs on αβ T cells proliferation, CD39$^+$γδ Tregs were sorted from patients with RSCRC/LSCRC and then were in vitro co-cultured with CD4$^+$/CD8$^+$ T cells isolated from PBMC of healthy volunteers in the presence of CD3 and CD28 mAbs. As shown in Figure 3B-E, tumor-infiltrating CD39$^+$γδ Tregs in RSCRC significantly inhibited both CD4$^+$/CD8$^+$ T cells proliferation and, as expected, their suppressive functions were stronger than that of LSCRC. Using the neutralizing antibody to suppress CD39 or blocking adenosine receptor signals both rescued the proliferation of αβ T cells. Also, CD39$^+$γδ Tregs in LSCRC and RSCRC both reduced the level of IFN-γ in CD8$^+$ T cells, and inhibiting CD39

rescued IFN-γ production (Figure 3F-G). Compared with LSCRC, the $CD39^+\gamma\delta$ Treg in RSCRC significantly suppressed the production of IFN-γ by $CD4^+$ T cells (Figure 3H-I). The function of Treg needs the continuous stimulation of various immunosuppressive cytokines and small molecule metabolites. Thus, we further explored whether adenosine level altered among different sites lead to the functional differences of $CD39^+\gamma\delta$ Tregs from LSCRC/RSCRC. As shown in Supplementary Figure 2, adenosine level was dramatically increased in ascending colon cancer (790.2 ± 178.9μM/L) than descending colon cancer (250.9 ± 78.7μM/L), sigmoid colon (173.0 ± 40.1μM/L), and rectal cancer (355.7 ± 83.8μM/L).

Given the substantial immunoregulatory function of $CD39^+\gamma\delta$ Tregs in RSCRC, we next analyzed the correlation between $CD39^+\gamma\delta$ Tregs expression and clinicopathological parameters of colorectal cancer. As shown in Table 1, the frequencies of tumor-infiltrating $CD39^+\gamma\delta$ Tregs were positively associated with lymph node metastasis and tumor stage (P=0.01). These findings suggest that tumor-infiltrating $CD39^+\gamma\delta$ Tregs contribute to tumor progression and the worse prognosis in RSCRC.

PLA2G4A/Arachidonic acid metabolic pathway was abnormally activated in RSCRC

To explore the molecular mechanism leading to the difference of $CD39^+\gamma\delta$ Tregs derived from RSCRC and LSCRC, we collected fresh tissue samples of stage III-IV RSCRC with high expression of $CD39^+\gamma\delta$ Tregs and the LSCRC with low expression of $CD39^+\gamma\delta$ Tregs detected by flow cytometry and identified 972 differential proteins by LC-MS based quantitative proteomic analysis with tandem mass tag (TMT) (Figure 4A). By analyzing KEGG pathway enrichment, we found that the high expression proteins in the RSCRC microenvironment were mainly concentrated in the metabolic pathway (Figure 4B). In contrast, the abnormal expression proteins in the LSCRC microenvironment were primarily involved in cell proliferation-related DNA replication and repair, transcription, translation, and protein folding (Figure 4B-C). According to these results, it is speculated that $CD39^+\gamma\delta$ $Tregs^{Low}$ LSCRC has stronger local proliferation ability and is more sensitive to anticancer drugs targeting cell growth signaling pathway compared to $CD39^+\gamma\delta$ $Tregs^{High}$ RSCRC. Notably, since the NCCN

guidelines in 2017 first proposed the difference in drug recommendation for RSCRC/LSCRC, NCCN guidelines for colorectal cancer diagnosis and treatment were updated again in 2019 (24): Cetuximab, an inhibitor of epidermal growth factor receptor, is no longer recommended for preoperative conversion therapy in patients with stage IV RSCRC (previously, the purpose of cetuximab preoperative treatment was to allow the tumor to shrink rapidly to obtain surgery opportunity). Clinical practice confirmed our results and conjectures. Besides, the proteins involved in the regulation of the immune system were predominantly expressed in RSCRC (RSCRC vs. LSCRC = 33 vs. 13, Figure 4C).

The considerable differences in the microenvironment of RSCRC and LSCRC raise an interesting question of how colorectal cells educate immune cells in the distinct microenvironment. By further analyzing the above quantitative proteomic results, we found that the calcium-dependent PLA2G4A/Arachidonic acid (AA) metabolic pathway was abnormally activated in RSCRC (Figure 4D-E). Meanwhile, the abnormally activated function of Fc gamma R-mediated phagocytosis in RSCRC (Figure 4B) is also dependent on the calcium pathway and PLA2/AA pathway (KEGG pathway: map04666). Phospholipase a2-IVa (PLA2G4A) is the most abundant subtype of cytosolic phospholipase A2 (cPLA2), which is a calcium-dependent protein. When cells are stimulated, specific transduction pathways regulate the increase of intracellular calcium concentration, and Ca^{2+} binds to the N-terminal C2 domain of cPLA2, which promotes the transfer of enzymes from the cytoplasm to the endomembrane (25). cPLA2 then hydrolyzes the acyl bond to produce arachidonic acid and lysophosphatidylcholine. Subsequently, arachidonic acid is converted into eicosanoid prostaglandins, leukotrienes, thromboxane, and other signaling lipid metabolites that may regulate T cell differentiation and trigger inflammatory responses (25). In addition, we analyzed the GEPIA2 analysis dataset and found that the expression levels of *PLA2G4A* in MSI-H (Microsatellite instability-high) colorectal tumors were significantly higher than that in MSI-L (Microsatellite instability-low) and MSS (Microsatellite stable) tumors (Figure 4F, MSI-H, n=48; MSI-L, n=48; MSS, n=175). These results indicate the value of PLA2G4A/AA

metabolism in exploring the immune microenvironment difference between RSCRC and LSCRC.

PLA2G4A induced the expression of CD39 on tumor-infiltrating γδ T cells

To elucidate whether overexpression of PLA2G4A in cancer cells activates the adenosine pathway of γδ T cells, we overexpressed *Pla2g4a* in the CT26 cell line. The overexpression was verified using qRT-PCR and Western Blot (Supplementary Figure 3A-C). Firstly, we ruled out the effect of overexpression of *Pla2g4a* itself on the growth and metastasis of CT26 cells (Supplementary Figure 3D-F). Then, CT26-*Pla2g4a* and CT26-Vec cells were cocultured with intraepithelial lymphocytes derived from the ileum (IL-IELs), colon (CO-IELs), or spleen of BALB/c mice. We observed the status of cells in the coculture system by fluorescence microscope after 12 and 36 hours, respectively, and found both IELs and splenocytes damage CT26-Vec to a great extent, while CT26-*Pla2g4a* inhibited the anti-tumor immune response (Figure 5A-D). On the other hand, lymphocytes were harvested at 12 and 36h respectively to detect the expression of CD39 on γδ T cells by flow cytometry. As expected, the overwhelming majority of γδ T cells cocultured with CT26-*Pla2g4a* were CD39 positive (Figure 5E-G). Consequently, the frequency of $CD39^+$ γδ Tregs increased 3.8-fold at 12 hours when compared with control (Figure 5H). Consistently, we observed similar results at 36 hours (Supplementary Figure 4A-D).

Furthermore, we identified a decreased cell number of CT26-Vec in as little as 2 hours after cocultured with γδ T cells sorted by magnetic beads (Figure 5I-J). In comparison, overexpressed *Pla2g4a* in CT26 cells weakened the anti-tumor immune response mediated by γδ T cells and induced the expression of CD39. Moreover, silencing *Pla2g4a* in CT26-*Pla2g4a* caused a reduction in CD39 expression on γδ T cells and rescued their function (Figure 5I-M). Moreover, $CD39^+$γδ Tregs induced by CT26-*Pla2g4a* predominately produced IL-17A (Supplementary Figure 4E).

To confirm the role of $PlA2G4A^{High}$ CRC on γδ T cells in vivo, we established an orthotopic murine model of colorectal cancer. As shown in Figure 6A-C, *Pla2g4a* upregulation

resulted in a substantial elevation of tumor weight and metastasis. All mice had bloody ascites in CT26-*Pla2g4a* groups. As expected, tumor-infiltrating γδ T cells isolated from the CT26-*Pla2g4a* group showed marked increases in the expression of CD39 when compared with control (Figure 6D-E), which is consistent with the results of coculture in vitro. In addition, the results of HE staining showed that the tumor invaded into the deep muscle layer (Figure 6F); on the other hand, it breaks through the serosal layer to achieve distal metastasis (Figure 6B and F), indicating that upregulation of *Pla2g4a* promotes tumor invasion.

To eliminate the interference of αβ T cells, we constructed a SCID mouse CRC orthotopic transplantation-adoptive transfer γδ T cell model (Figure 6G). Similarly, *Pla2g4a* upregulation promoted tumor progression (Figure 6H-I) and induced the expression of CD39 on tumor-infiltrating γδ T cells (Figure 6J-K).

These data collectively reveal a role for PLA2G4A^{High} CRC in the activation of the CD39/adenosine pathway in tumor-infiltrating γδ T cells, thereby promoting tumor progression and metastasis.

Exogenous AA induced CD39^{+}γδ Tregs polarization

Because PLA2G4A catalyzes AA production from phospholipids, we further explored whether AA treatment could induce CD39^{+}γδ Tregs polarization in vitro. As shown in Figure 7A-F, AA promoted the expression of CD39 on γδ T cells and decreased IFN-γ intracell production. Further, we sorted the AA-induced-CD39^{+}γδ Tregs and determined the immunosuppressive function. Consistent with the results of RSCRC, AA-induced-CD39^{+}γδ Tregs significantly inhibited the proliferation of CD8^{+}T cells (Figure 7G-H). Moreover, neutralization of CD39 by an antibody or blocking the high-affinity adenosine 2A receptor (A2AR) signaling rescued cell proliferation (Figure 7G-H), confirming that CD39-adenosine is leading to the immunosuppression of CD39^{+}γδ Tregs.

PLA2G4A shortened the survival of patients with RSCRC

To evaluate the role of PLA2G4A in human colorectal cancer, we determined PLA2G4A expression by immunohistochemistry in 94 patients with different histological grades of colorectal cancer. Interestingly, clinical survival analysis indicated that the III-IV stage RSCRC patients with low PLA2G4A expression level had a better outcome in overall survival (P=0.04) (Figure 8A), whereas a low-PLA2G4A expression indicated poor prognosis in LSCRC (P=0.01) (Figure 8B). There was no noticeable difference in overall survival between the two groups without distinguishing the tumor site (Figure 8C). We also observed no difference in overall survival between the two groups in patients with stages I to IV CRC (Supplementary Figure 5).

Clinicopathological analysis showed that PLA2G4A expression was positively correlated with the expression of γδ TCR, CD8 and PD-1(γδ TCR, R=0.704, P=0.01; CD8, R=0.503, P=0.024; PD-1, R=0.577, P=0.008) in stage III-IV RSCRC. γδ TCR (P=0.01), CD8 (P=0.021) and PD-1 (P=0.003) were upregulated in PLA2G4A^{high} cohort (Table 2, Figure 8D). Similarly, the rate of PD-1 expression was significantly increased in stage I-IV RSCRC with high expression of PLA2G4A (P=0.017, Table 3). Among the 34 cases of PD-1 negative patients, 18 (52.9%) were PLA2G4A^{high} expression, whereas, among the 12 cases of PD-1 positive patients, 11 (91.7%) were PLA2G4A^{high} expression (Table 3). These results highlight the potential of PLA2G4A in predicting and evaluating the immune microenvironment of such patients. Consistently, we also observed increased infiltration of CD8^{+}T cells and elevated expression of PD-1 in the CT26-*Pla2g4a* mice (Supplementary Figure 6). On the other hand, we did not observe the correlation between PLA2G4A and PD-1 in LSCRC (Supplementary Table 1). Thus, these clinical data in human samples suggest that the expression of PLA2G4A alters in LSCRC/RSCRC and support our experimental conclusions.

In addition, we analyzed the ImmuCellAI analysis dataset and found that the infiltration of γδ T cells in both COAD and READ were significantly increased compared to normal tissues (Figure 8E-F; COAD, n=288, Normal, n=40; READ, n=95, Normal, n=10), while CD4^{+}T cells were decreased (Figure 8G-H). Compared with normal tissues, the infiltration of CD8^{+}T cells

decreased in COAD (Figure 8I). There was no difference in $CD8^+$T cells between the tumor and normal tissues in the rectum (Figure 8J). These data implicated that γδ T cells may play a more critical role than αβ T cells in mediating the tumor-specific immune response in the human CRC microenvironment, highlighting the transformation of γδ T cells into $CD39^+$γδ Tregs itself promotes tumor immune escape.

Taken together, the above results revealed that RSCRC recruits γδ T cells and induces $CD39^+$γδ Tregs polarization through PLA2G4A/AA pathway. On the one hand, the anti-tumor effect mediated by γδ-TIL is greatly reduced. On the other hand, $CD39^+$γδ Tregs further weaken the immune function of αβ T cells via adenosine, thus promoting tumor progression.

Discussion

In the present study, we aimed to define the distribution and function characteristics of $CD39^{+}\gamma\delta$ Tregs in human RSCRC and LSCRC. Besides the known differences in cancer cells themselves, our finding highlights the domestication of immune cells by distinct molecular subtypes of cancer; in return, tumor-educated immunosuppressive cells facilitate tumor progression. Specifically, we demonstrated that the frequency of TIL $CD39^{+}\gamma\delta$ Tregs is greatly increased in RSCRC with abnormal activation of PLA2G4A/AA pathway, along with upregulation of IL-17A and adenosine, consequently enhanced immunosuppressive function. We discovered unexpectedly that high expression of PLA2G4A suggested poor prognosis in RSCRC. While for LSCRC, relatively "cold" tumors, the upregulation of PLA2G4A prolonged survival. These observations indicate the significance of studying the crosstalk between cancer cells and immune cells by distinguishing the primary tumor site and offering precise clinical treatment insights.

The critical problem that restricts immunotherapy application in colorectal cancer is that it is difficult for immune cells to enter the local tumor. We hope to make a breakthrough in immunotherapy of colorectal cancer by restoring the anti-tumor immune response of effector T cells resident in intestinal epithelial tissue. The γδ T cells in the colon are vital to the first line of defense in intestinal tissue immune surveillance (26). The γδ T cells in this organ are composed of resident and infiltrating cells. The resident subsets are called intraepithelial lymphocytes (IEL). γδ IELs account for 30% and 50% of IELs in humans and mice, respectively, (27, 28). γδ T cells can not only dissolve cancer cells directly through the perforin granzyme pathway (29, 30) but also interact with B cells, DC cells, αβ T cells, and NK cells respectively to play an indirect anti-tumor effect （31). Compared with αβ T cells, γδ T cells are more likely to migrate into other tissues (31) and can

quickly respond to targets and release effector cytokines, such as IFN-γ (32). More importantly, γδ T cells have higher invasive ability and function in tumor hypoxia environment (30). Therefore, γδ T cells are very advantageous candidate cells in tumor immunotherapy. However, recent researches demonstrated that tumor-educated γδ T cells could function in suppressing anti-tumor immunity. A previous study indicates that the γδ T cells could be domesticated by colorectal cancer and polarize to $CD39^{+}$γδ Tregs, and play an immunosuppressive role by secreting adenosine. We also observed the above phenomenon here, but the primary tumor site on cell interaction in the microenvironment has not been elucidated. Here, our data showed a higher accumulation of tumor-infiltrating $CD39^{+}$γδ Tregs in RSCRC than paired normal tissue and LSCRC, along with increased production of IL-17A and adenosine and upregulation of Tim-3. By comparing T cells in fresh tissues of patients with double primary colorectal cancer, we found that $CD39^{+}$γδ Tregs from the RSCRC exert stronger immunosuppressive ability than LSCRC.

In order to apply the γδ T cell in the immunotherapy of solid tumor, it is necessary to prevent γδ T cell from mutiny after entering the tumor microenvironment. Therefore, it is urgent to study the pathway of tumor-inducing γδ Tregs thoroughly. Despite a large focus of tumor-educated γδ Tregs research centered on TGFβ and its related signaling pathway (14, 33-35), we did not find the difference of TGFβ pathway in colorectal cancer with $CD39^{+}$γδ $Tregs^{Low}$ and $CD39^{+}$γδ $Tregs^{High}$ by proteomic analysis. We further found that PLA2G4A/AA pathway was abnormally activated in RSCRC with high expression of $CD39^{+}$γδ Tregs. Notably, this pathway is involved in a number of abnormal activations signaling pathways and biological functions of RSCRC. The involvement of the PLA2G4A/AA pathway in the inflammatory process and T cell polarization has been confirmed

by many studies (36-39). Prostaglandin E2 (PGE2) produced by cyclooxygenase (COX) catalyzing AA can induce Th17 production in intestinal mucosa by enhancing IL-23 signal (36, 37), while PGE2 can induce $CD4^{+}Foxp3^{+}$T cells in mesenteric lymph nodes (38). ALOX15 catalyzes AA to 15s-HpETE, which in turn promotes the transformation of immature $CD4^{+}$ T cells into T helper follicular cells (39). Therefore, we further study and confirm that overexpression of PLA2G4A induced the activation of the CD39/adenosine pathway in γδ T cell to impair its anti-tumor response, consequently promoting tumor progression. Besides, a large amount of PGE2 released by pancreatic ductal adenocarcinoma cells with upregulation of COX2 impairs γδ T cell cytotoxicity (40). However, we did not discover a difference in COX2 expression in colorectal cancer with $CD39^{+}$γδ $Tregs^{Low}$ and $CD39^{+}$γδ $Tregs^{High}$. Interestingly, 15-LOX increased in the latter (Figure 3). Therefore, we speculate that CRC with PLA2G4A/AA abnormal activation may induce $CD39^{+}$γδ Tregs through the downstream lipoxygenase pathway. Further exploration is needed to confirm the above hypothesis. Moreover, it is also possible that the cancer cells secrete more AA to the extracellular, and metabolites of AA in the γδ T cells induce the expression of CD39. We initially explored this possibility and found that γδ T cells treated with AA in vitro showed increased CD39 expression, decreased intracellular IFN-γ, and ability to inhibit the proliferation of $CD8^{+}$T cells (Figure 6). More research is needed to determine which way works.

Notably, γδ-TILs from CRC patients were dominantly tissue-resident Vδ1 subset rather than circulating Vδ2 subset (Supplementary Figure 1). Therefore, instead of simply constructing a subcutaneous tumor model, we inoculated CT26 cells into the intestinal wall of mice to mimic the effect of CRC on the intestinal resident γδ T cells. Although human and mouse γδ T cell subsets are

not homologous, they are both intestinal resident γδ T cells, and the induction effects of tumors on these cells are similar. To explore the interaction between CRC and tissue-resident γδ T cells, the mouse models used in this study are currently a relatively feasible and appropriate solution.

Previous studies have suggested that the left- and right-sided large intestine have different immune environments, leading to the distinct immune responses to stimulation (41). The size and number of submucosal isolated lymphoid follicles (SM-ILFs), which comprise a central follicle of B cells surrounded by T cells, in the right large intestine are larger than those in the left large intestine. Interestingly, SM-ILFs are the main adaptive immune inductive sites of the cecum and proximal and transverse colon (right-sided), whereas mucosal isolated lymphoid follicles (M-ILFs) serve such functions in the ileum and distal colon (left-sided) (41). Based on the biology of the disease, consensus molecular subtypes (CMSs) divides CRCs into one of four CMS groups: CMS1, microsatellite instability (MSI) immune; CMS2, canonical; CMS3, metabolic; and CMS4, mesenchymal (42). CMS1 is mainly RSCRC, while CMS1 proportion in LSCRC is only 9.01% (31/344) (43, 44). According to the above mechanism study results and clinical studies, we speculate that the right-sided large intestine may have more abundant immune cells. When the level of PLA2G4A increases, $CD39^{+}$γδ Tregs would be induced to form an immunosuppressive microenvironment and promote tumor progression (the present study provided relevant evidence). However, gut-associated lymphoid tissues (GALTs) of the left-sided large intestine are not rich enough. The inflammatory response mediated by the PLA2G4A/AA signaling pathway may help recruit immune cells, thus enhancing the immune response. This may be why the expression of PLA2G4A has different effects on the survival of patients with RSCRC/LSCRC. In addition,

according to our results of flow cytometry and proteomics, the $CD39^{+}\gamma\delta$ $Tregs^{Low}$ LSCRC belongs to CMS2 while $CD39^{+}\gamma\delta$ $Tregs^{High}$ RSCRC is similar to CMS1. There is a great difference in the domestication of γδ T cells by the two types of tumors, which is certainly not fully explained by one pathway. From the perspective of immune cells, the function of Treg needs the continuous stimulation and maintenance of various immunosuppressive cytokines and small molecule metabolites. Our results showed that the adenosine level in RSCRC was significantly higher than that of LSCRC, suggesting that the microenvironment of different sites affected the immune regulation function of $CD39^{+}\gamma\delta$ Tregs. All of these factors may contribute to the difference in overall survival. Further studies and larger samples are needed to confirm this hypothesis.

In summary, the present study indicates that the RSCRC microenvironment with abnormal activation of PLA2G4A educated γδ T cells into $CD39^{+}$ γδ Tregs, which produce the pro-tumor cytokine IL-17A and adenosine, consequently, establish a potent immunosuppressive microenvironment for promoting immune evasion and tumor metastasis. Our work revealed $CD39^{+}$ γδ Tregs as a critical factor correlated with the progression of $PLA2G4A^{high}$ RSCRC and deepen the understanding of tumor microenvironment and immunosuppression.

Methods

Patient tissue samples

A total of 129 patients with CRC who were admitted and treated at Tianjin Medical University Cancer Institute and Hospital between February 2014 and September 2020 were enrolled randomly. During surgical resection, specimen (both tumor and paired normal tissues) were obtained from the treatment-naïve patients with CRC. The clinical features of the patients are presented in Table I. The records of all of the patients contained basic information, including Tumor-Node-Metastasis (TNM) stage, the degree of differentiation, lymph node metastasis and distant metastasis, according to the 2002 International Cancer Alliance TNM staging criteria (45).

Isolation of tissue-infiltrating cells

Fresh colorectal tumor tissues and paired normal tissues from patients with CRC were prepared by mechanical disruption, followed by digestion with 0.5 mg/ml collagenase type IV (cat. no. C5138; Sigma-Aldrich) in 10% FBS with 10 U/ml DNase I in RPMI-1640 medium (both from Gibco; Thermo Fisher Scientific) at 37˚C for 30 min. Digested tissues were incubated for 5 min at 37˚C with EDTA (0.5 M) to prevent dendritic cell/T-cell aggregation and filtered through a 100-µm and a 40-µm filter. The isolation and culture of tissue/tumor-infiltrating cells were performed as previously described (46).

For $CD39^{+}\gamma\delta$ Tregs functional experiments, single-cell suspensions from tissues were generated rapidly and gently using the Tumor Dissociation Kit (cat. no.130-095-929; Miltenyi Biotec) and gentleMACS Octo Dissociator (cat. no. 130-095-937; Miltenyi Biotec).

Flow cytometric analysis.

Tumor/paired normal tissue-infiltrating cells ($1x10^6$ cells) were incubated with human PerCP anti-CD45 mAb (1:20; cat. no. 304026; BioLegend), FITC anti-CD3 mAb (1:20; cat. no. 300452; BioLegend), APC anti-CD4 mAb (1:20; cat. no. 357408; BioLegend), APC anti-CD8 mAb (1:20; cat. no. 344722; BioLegend), APC anti-TCR γ/δ mAb (1:20; cat. no. 331212; BioLegend), FITC anti-TCR Vδ1 mAb (1:25; GTX79223; GeneTex), PE anti-human TCR Vδ2 (1:20; cat. no. 331408;

BioLegend), PE anti-CD39 mAb (1:20; cat. no. 328208; BioLegend), APC/Cy7 anti-PD-1 mAb (1:20; cat. no. 329921; BioLegend), and PE/Cy7 anti-T-cell immunoglobulin mucin family member 3 (Tim-3) mAb (1:20; cat. no. 345013; BioLegend) in cell staining buffer (cat. no. 420201; BioLegend) for 15 min at RT. For intracellular staining, cells were incubated with PE/Cy7 anti-IFN-γ mAb (1:20; cat. no. 502527; BioLegend) and APC/Cy7 anti-IL17A mAb (1:20; cat. no. 512334; BioLegend) in 100μl intracellular staining permeabilization buffer (cat. no. 421002; BioLegend) for 15 min at RT. LIVE/DEAD Fixable Dead Cell Stain Kits (cat. no. L34963; Invitrogen) were used to stain dead cells. After washing with PBS and centrifugation at 400 x g for 5 min at 4˚C, $1x10^6$ cells were suspended in 300 μl cell staining buffer (cat. no. 420201; BioLegend) and analyzed on a BD FACSCalibur (BD Biosciences) flow cytometer. The data were analyzed using FlowJo v10 software (FlowJo, LLC).

For mouse experiment, FITC anti-CD3 mAb (1:20; cat. no. 100204; BioLegend), APC anti-TCR γ/δ mAb (1:20; cat. no. 118116; BioLegend), PE anti-CD39 mAb (1:20; cat. no. 143804; BioLegend), APC anti-CD8a mAb (1:20; cat. no. 100712; BioLegend), APC anti-CD4 mAb (1:20; cat. no. 100412; BioLegend), PE/Cy7 anti-IFN-γ mAb (1:20; cat. no. 505826; BioLegend), and APC/Cy7 anti-IL-17A mAb (1:20; cat. no. 506940; BioLegend) were used for staining and detected by flow cytometry.

Extracellular adenosine detection

Adenosine concentrations were measured using a high-performance liquid chromatography (HPLC) system equipped with an Inertsil ODS-SP C18 chromatogram column (4.6 mm x 250 mm, 5 mm, Japan) using a mobile phase consisting of methanol and 0.05 M potassium dihydrogen phosphate at the volume ratio of 10: 90. Identification and quantification of adenosine peaks were done by comparison to retention times of known standards (cat. no. 123179-97-5; Selleck) and peak integration and normalization.

In vitro suppressive assay

For $CD39^+\gamma\delta$ Tregs mediated $CD4^+/CD8^+$T-cell suppression experiment, $CD39^+$ γδ Tregs were sorted from tumors and paired normal tissues of RSCRC/LSCRC patients, and then were co-cultured with allogeneic peripheral blood CFSE (5μM; cat. no. 65-0850-84; Invitrogen)-labeled $CD4^+/CD8^+$T cells at a 1:5 ratio in the presence of ImmunoCult™ Human CD3/CD28 T Cell Activator (cat. no. 10971; Stemcell Technologies) for 5 days. An anti-CD39 mAb (5μg/ml; ab178572; Abcam) and an A2AR inhibitor, AZD4635 (5μM; M7531; AbMole), were used for rescue experiments. $CD4^+/CD8^+$T cells were separated by RosetteSep Human $CD4^+$T Cells Enrichment Cocktail (cat. no. 15062; Stemcell Technologies) and an EasySep Direct Human $CD8^+$T Cell Isolation Kit (cat. no. 19663; Stemcell Technologies). On day 5, cells were harvested and intracellularly stained with anti-IFN-γ mAb. CFSE-low cells and IFN-γ production were detected by flow cytometry. Peripheral blood samples of the healthy donor were collected in Tianjin Medical University Cancer Institute and Hospital.

Tandem Mass Tag (TMT) proteome analysis

We selected 6 samples of $CD39^+$ γδ $Tregs^{High}$ RSCRC and $CD39^+$ γδ $Tregs^{Low}$ LSCRC for proteomic characterization using TMT (Thermo Fisher Scientific). After protein extraction, the whole protein in tissue cells was obtained. The whole protein was hydrolyzed into peptides by trypsin, and all peptides were labeled by TMT reagent. The labeled peptides of each group were mixed and graded by Agilent 1260 infinity II HPLC system. Buffer A was 10 mm hcoonh4, 5% ACN, pH 10.0, and buffer B was 10 mm hcoonh4, 85% ACN, pH 10.0. The chromatographic column was equilibrated with liquid A. Samples were loaded into the chromatographic column by the manual automatic injector for separation. The flow rate was 1ml/min. Collect the eluting components. Lyophilized and then redissolved samples with 0.1% FA. Each sample was separated by Easy nLC system (Thermo Fisher Scientific), and then analyzed by Q Exactive plus mass spectrometer (Thermo Fisher Scientific).

Proteome discoverer 2.1 (Thermo Fisher Scientific) software transformed the original atlas file generated by Q Exactive plus into a .mgf file, which was submitted to the MASCOT2.6 server for database retrieval through the built-in tool of the software. Then the database search file (. dat file)

formed on the MASCOT server was sent back to the software through the proteome discoverer 2.1, and the data was filtered according to the FDR < 0.01 standard to obtain highly reliable qualitative results. The database used in this study was: Uniprot_HomoSapiens_20386_20180905.

Analysis of public datasets.

RNA sequencing-based gene expression data in CRC was obtained from the Gene Expression Profiling Interactive Analysis (GEPIA) database (47) and ImmuCellAI analysis dataset (48) for cancer genomics. For gene expression, P<0.01 was used as the cut-off.

Lentivirus construction and stable cell line establishment

The mouse *Pla2g4a* gene was amplified by PCR with primers 5'-AGGTCGACTCTAGAGGATCCCGCCACCATGTCTTTCATAGATCCTTATCAGCAC-3' (forward) and 5'-TCCTTGTAGTCCATACCCACAGTGGGTTTACTTAGAAACTC-3' (reverse). Next, the PCR products were inserted into the BamH I and Agel sites of GV492 vector (Genechem Co.,Ltd, Shanghai, China). Lentiviruses were produced by 293T cells for stable transfection of cell lines, following the manufacturer's instructions. Empty vector was transfected into the cells as a control. A total of 1×10^5 CT26 cells in 1ml 1640 medium with 4ug/ml polybrene were infected with 2×10^6 TU/ml lentivirus. After 48h, 3ug/ml puromycin was added for selection. The *Pla2g4a* overexpression cells (CT26-*Pla2g4a*) and control cells (CT26-Vec) were observed and photographed by fluorescence microscope (Supplementary Figure 3A). Transfection efficiency was determined by real-time PCR and western blot (Supplementary Figure 3B and C). CT26 and 293T cells were purchased from American Type Culture Collection (ATCC, Manassas, VA, USA).

RNA isolation and real-time quantitative PCR (qRT-PCR)

Total RNA was extracted from cell lines using an RNApure Tissue&Cell Kit (Cwbiotech, Beijing, China) following the manufacturer's protocol. qRT-PCR for mRNAs were performed as described previously with primers *Pla2g4a* 5'-AAAAGAGTACCAAAGCGACAAC-3' (forward)

and 5’-CGTCCTTCTCGGGTATTGAATA-3’(reverse) (49). Commercial mouse *Gapdh* (cat. no. B661304, Sangon Biotech, Shanghai, China) was used as the internal control.

siRNA and transfection

Small interfering RNA (siRNA) was used for transient knockdown of *Pla2g4a*. *Pla2g4a* siRNA (cat. no. sc-35098) and control siRNA (cat. no. sc-37007) were purchased from the Santa Cruz Biotechnology (Santa Cruz, CA, USA) and used at a final concentration of 100 nmol/L. The cells were transfected using siRNA transfection reagent (cat. no. sc-29526) according to the manufacturer’s instructions.

Isolation of Intraepithelial lymphocytes

Separate the mouse ileum and colon, remove Peyer's Patches and the intestinal contents with PBS. Place the isolated intestine into cold RPMI-1640 containing 10% FBS to maximize cell viability. Cut the intestine open and cut into 1 cm segments. Incubated the segments in 30 ml RPMI containing 93 μl 5% (w/v) dithiothreitol (DTT) + 60 μl 0.5 M EDTA + 500 μl FBS, stir at 500 rpm for 15 min at 37 °C. Filter digested tissue through a 100 μm cell strainer. Rinse the strainer with 20 ml of RPMI-1640 containing 10% FBS. Collect the cells in the filtration and suspend it with 3ml 40% Percoll solution, mix well and gently superimpose it on 2ml 70% Percoll solution, centrifuge at 600g for 20min to collect the cells.

In vitro CD39$^+$ γδ Tregs induction by cancer cells

Intraepithelial lymphocytes derived from the ileum (IL-IELs), colon (CO-IELs), or spleen of BALB/c mice were co-cultured with CT26-Vec or CT26-*Pla2g4a* for 12 and 36 hours (IELs:CT26=1:4). For rescue experiments, γδ T cells sorted from IELs of BALB/c mice were co-cultured with CT26-Vec or CT26-*Pla2g4a* (γδ T:CT26=1:1) with siRNA pretreatment for 2 hours using a mouse TCRγ/δ T cell Isolation Kit (cat. no. 130-092-125; Miltenyi Biotec). An anti-Pla2g4a antibody (5 μg/ml; cat. no. 110218; GeneTex) was used to neutralize PLA2G4A in cell culture

supernatant. And then cells were washed, harvested, and then stained with PE anti-CD39 mAb (1:20; cat. no. 143804; BioLegend) and detected by flow cytometry.

Orthotopic murine model of colorectal cancer

Six- to eight-week-old male BALB/c mice or SCID mice were purchased from SPF Biotechnology Co., Ltd. (Beijing, China) and used for animal studies. CT26-Vec/-*Pla2g4a* cells ($1x10^7$) were suspended in 100μL PBS containing 33ul Matrigel (cat. no. 354234, Corning), then cells were surgically transplanted into the submucosa of the caecal wall of a BALB/c mouse or a SCID mouse. The cecum was exteriorized through a midline abdominal incision and cells was surgically transplanted in the caecal submucosa. Matrigel keeps the cells in place, allowing them to engraft and expand in the cecal wall. Over time, matrigel is degraded and the engrafted CT26 cells remains. Approximately 3-4 weeks after transplantation, the presence of primary tumors could be detected by abdominal palpation. Then the BALB/c mice were sacrificed and the orthotopic tumor, intestinal metastasis and distal organ metastasis were obtained. For SCID mice experiments, adoptive transferred γδ T cells ($5x10^6$) derived from BALB/c mice 7 days after transplantation. Two weeks after adoptive transfer, the SCID mice were sacrificed.

In vitro $CD39^+$ γδ Tregs induction by AA

Naïve γδ T cells sorted from splenocytes of BALB/c mice were treated with AA (5μM, cat. no. A5837; Sigma-Aldrich) using a mouse TCRγ/δ T cell Isolation Kit (Miltenyi Biotec) for 12 and 36 hours. And then cells were washed, harvested, and then stained with PE anti-CD39 mAb or intracellular stained with PE-Cy7 anti-IFN-γ mAb (1:20; cat. no. 505826; BioLegend) and detected by flow cytometry.

For AA-induced-$CD39^+$γδ Tregs mediated $CD8^+$T-cell suppression experiment, $CD39^+$ γδ Tregs were sorted from above γδ T cells pretreated with AA (5μM), and then were co-cultured with αβ T cells labeled CFSE (Invitrogen) at a 1:5 ratio for 2 days. αβ T cells were unlabeled by magnetic beads in the process of sorting γδ T cells. An anti-CD39 mAb (5μg/ml; ab227840; Abcam) and an A2AR inhibitor, AZD4635 (5μM; M7531; AbMole), were used for rescue experiments. And then

cells were washed, harvested, and then stained with APC anti-CD8 mAb (1:20; cat. no. 100712; BioLegend). CFSE-low $CD8^+$T cells were detected by flow cytometry.

Immunohistochemistry (IHC)

Colorectal tumor tissues and normal control tissues were fixed with 4% formaldehyde for 24 h at room temperature (RT), embedded in paraffin and cut into 4-μm sections. The sections were dewaxed with xylene then hydrated through a graded series of ethanol for 5 min in each percentage at RT. Slides were boiled in 10 mM sodium citrate buffer pH 6.0 at 95˚C for 10 min and subsequently incubated in 3% hydrogen peroxide for 10 min. Sections were blocked with 100-400 μl 5% normal goat serum in TBS-Tween (cat. no. 5425; Cell Signaling Technology) for 1 h at RT. To assess PLA2G4A/CD8/PD-1/γδ TCR expression in the CRC specimens, sections were incubated with an anti-PLA2G4A antibody (dilution, 1:100; cat. no. sc-454; Santa Cruz) or an anti-CD8 antibody (dilution, 1:200; cat. no. 85336; Cell Signaling Technology) or an anti-PD-1 antibody (dilution, 1:200; cat. no.86163; Cell Signaling Technology) or an anti-γδ TCR antibody ((dilution, 1:100; cat. no.331202; Biolegend) overnight at 4˚C, and were then incubated with a horseradish peroxidase-conjugated secondary antibody (dilution, 1:1,000; cat. no. ab6721; Abcam) at room temperature for 1 h. Following washing with PBS, the sections were incubated for 30 min at RT with streptavidin-biotin conjugated with horseradish peroxidase [dilution, 1:100; cat. no. KIT-0305; UltraSensitive™ SP (Mouse/Rabbit) IHC kit]. Subsequently, the slides were stained with 3,3'-diaminobenzidine (Fuzhou Maixin Biotech Co., Ltd.), and the nuclei were counterstained with haematoxylin for 5 min at RT. Morphometric analyses of the tumor and paired normal tissues were performed using an Olympus BX51 light microscope (magnification, x20; Olympus Corporation). Images were obtained from 10 randomly selected areas.

Staining score was calculated by multiplying percentage of positive cells with staining and intensity of staining. Staining intensity was scored as follows: 0, Negative; 1, weakly positive; and 2, positive. According to the percentage of cancer cells per the whole tumor area: 0 (0%), 1 (< 25%), 2 (26%-50%), 3 (51% -75%), and 4 (>75%). Samples were subsequently grouped into Low expression and high expression groups. Median level was used as cutoff.

Statistics

Statistical analysis was performed using GraphPad Prism v8 software (GraphPad Software, Inc.). Data are presented as the mean ± standard error of the mean of three repeats. A $\chi 2$ test was used to evaluate the association between PLA2G4A expression and the clinicopathological parameters. A log-rank test was used to compare the survival curves of two groups. Two-way ANOVA followed by Sidak's multiple comparison test was used for multiple-group analyses. Pearson correlation analysis was used to analyze the correlation between the expression of PLA2G4A and the pathological grade or TNM stage. $P<0.05$ was considered to indicate a statistically significant difference.

Study approval

All the samples were collected according to standard local protocols and after obtaining informed consent. The Ethics Committee from Tianjin Medical University Cancer Institute and Hospital provided approval for the study. The procedures for the handling and care of the mice were approved by the Animal Experimentation Ethics Committee of Tianjin Medical University Cancer Institute and Hospital.

Author contributions

DK and YZ designed research studies. DK and TZ provided financial support and supervised the study. YZ conducted experiments, acquired data and wrote the manuscript. LZ, DH, JW, and KL assisted with the collection and treatment of surgical specimens. JL and JG analyzed the data. All authors participated in the interpretation of data and editing of the manuscript for intellectual content. All authors approved the final manuscript.

Acknowledgments

This research was funded by the National Natural Science Foundation of China (No. 81672884) and the National Science and Technology Major Project of China (No. 2017ZX10203207-004-005).

This research was also funded by the Science & Technology Development Fund of Tianjin Education Commission for Higher Education, grant number 2017KJ204 and 2020KJ133.

We thank Shaolan Zou and Fengmin Jin (School of chemical engineering and technology, Tianjin University) for the flow cytometry sorting experiment assistant.

References

1. Siegel RL, et al. Cancer Statistics, 2021. *CA Cancer J Clin.* 2021;71(1):7-33.
2. DeSantis CE, et al. Cancer treatment and survivorship statistics, 2014. *CA Cancer J Clin.* 2014;64(4):252-71.
3. Le DT, et al. PD-1 Blockade in Tumors with Mismatch-Repair Deficiency. *N Engl J Med.* 2015;372(26):2509-20.
4. Croci DO, et al. Dynamic cross-talk between tumor and immune cells in orchestrating the immunosuppressive network at the tumor microenvironment. *Cancer Immunol Immunother.* 2007;56(11):1687-700.
5. von Einem JC, et al. Left-sided primary tumors are associated with favorable prognosis in patients with KRAS codon 12/13 wild-type metastatic colorectal cancer treated with cetuximab plus chemotherapy: an analysis of the AIO KRK-0104 trial. *J Cancer Res Clin Oncol.* 2014;140(9):1607-14.
6. Price TJ, et al. Does the primary site of colorectal cancer impact outcomes for patients with metastatic disease? *Cancer.* 2015;121(6):830-5.
7. Cai X, et al. Correlation of multiple proteins with clinic-pathological features and its prognostic significance in colorectal cancer with signet-ring cell component. *Eur Rev Med Pharmacol Sci.* 2016;20(16):3358-67.
8. Brule SY, et al. Location of colon cancer (right-sided versus left-sided) as a prognostic factor and a predictor of benefit from cetuximab in NCIC CO.17. *Eur J Cancer.* 2015;51(11):1405-14.
9. Loupakis F, et al. Primary tumor location as a prognostic factor in metastatic colorectal cancer. *J Natl Cancer Inst.* 2015;107(3).
10. Moretto R, et al. Location of Primary Tumor and Benefit From Anti-Epidermal Growth Factor Receptor Monoclonal Antibodies in Patients With RAS and BRAF Wild-Type Metastatic Colorectal Cancer. *Oncologist.* 2016;21(8):988-94.
11. Kibble A, et al. Highlights from the 52nd Annual Meeting of the American Society of Clinical Oncology (ASCO) (June 3-7, 2016 - Chicago, Illinois, USA). *Drugs Today (Barc).* 2016;52(7):407-23.
12. Shida D, et al. Prognostic Value of Primary Tumor Sidedness for Unresectable Stage IV Colorectal Cancer: A Retrospective Study. *Ann Surg Oncol.* 2019;26(5):1358-65.
13. Benson AB, 3rd, et al. Colon Cancer, Version 1.2017, NCCN Clinical Practice Guidelines in Oncology. *J Natl Compr Canc Netw.* 2017;15(3):370-98.
14. Hu G, et al. Tumor-infiltrating CD39(+)gammadeltaTregs are novel immunosuppressive T cells in human colorectal cancer. *Oncoimmunology.* 2017;6(2):e1277305.
15. Weis SM, Cheresh DA. Tumor angiogenesis: molecular pathways and therapeutic targets. *Nat Med.* 2011;17(11):1359-70.
16. Kashyap AS, et al. Antisense oligonucleotide targeting CD39 improves anti-tumor T cell immunity. *J Immunother Cancer.* 2019;7(1):67.
17. Cekic C, Linden J. Adenosine A2A receptors intrinsically regulate CD8+ T cells in the tumor microenvironment. *Cancer Res.* 2014;74(24):7239-49.
18. Silva-Santos B, et al. gammadelta T cells in cancer. *Nat Rev Immunol.* 2015;15(11):683-91.
19. Wu P, et al. gammadeltaT17 cells promote the accumulation and expansion of myeloid-

derived suppressor cells in human colorectal cancer. *Immunity.* 2014;40(5):785-800.
20. Coffelt SB, et al. IL-17-producing gammadelta T cells and neutrophils conspire to promote breast cancer metastasis. *Nature.* 2015;522(7556):345-8.
21. Ma S, et al. IL-17A produced by gammadelta T cells promotes tumor growth in hepatocellular carcinoma. *Cancer Res.* 2014;74(7):1969-82.
22. Anderson AC, et al. Lag-3, Tim-3, and TIGIT: Co-inhibitory Receptors with Specialized Functions in Immune Regulation. *Immunity.* 2016;44(5):989-1004.
23. Khalil DN, et al. The future of cancer treatment: immunomodulation, CARs and combination immunotherapy. *Nat Rev Clin Oncol.* 2016;13(5):273-90.
24. Gupta S, et al. NCCN Guidelines Insights: Genetic/Familial High-Risk Assessment: Colorectal, Version 2.2019. *J Natl Compr Canc Netw.* 2019;17(9):1032-41.
25. Leslie CC. Cytosolic phospholipase A(2): physiological function and role in disease. *J Lipid Res.* 2015;56(8):1386-402.
26. Di Marco Barros R, et al. Epithelia Use Butyrophilin-like Molecules to Shape Organ-Specific gammadelta T Cell Compartments. *Cell.* 2016;167(1):203-18 e17.
27. Pang DJ, et al. Understanding the complexity of gammadelta T-cell subsets in mouse and human. *Immunology.* 2012;136(3):283-90.
28. Edelblum KL, et al. Dynamic migration of gammadelta intraepithelial lymphocytes requires occludin. *Proc Natl Acad Sci U S A.* 2012;109(18):7097-102.
29. Corvaisier M, et al. V gamma 9V delta 2 T cell response to colon carcinoma cells. *J Immunol.* 2005;175(8):5481-8.
30. Meraviglia S, et al. Distinctive features of tumor-infiltrating gammadelta T lymphocytes in human colorectal cancer. *Oncoimmunology.* 2017;6(10):e1347742.
31. Suzuki T, et al. Gut gammadelta T cells as guardians, disruptors, and instigators of cancer. *Immunol Rev.* 2020;298(1):198-217.
32. Halary F, et al. Shared reactivity of V{delta}2(neg) {gamma}{delta} T cells against cytomegalovirus-infected cells and tumor intestinal epithelial cells. *J Exp Med.* 2005;201(10):1567-78.
33. Ni C, et al. Breast cancer-derived exosomes transmit lncRNA SNHG16 to induce CD73+gammadelta1 Treg cells. *Signal Transduct Target Ther.* 2020;5(1):41.
34. Li X, et al. Generation of human regulatory gammadelta T cells by TCRgammadelta stimulation in the presence of TGF-beta and their involvement in the pathogenesis of systemic lupus erythematosus. *J Immunol.* 2011;186(12):6693-700.
35. Casetti R, et al. Cutting edge: TGF-beta1 and IL-15 Induce FOXP3+ gammadelta regulatory T cells in the presence of antigen stimulation. *J Immunol.* 2009;183(6):3574-7.
36. Boniface K, et al. Prostaglandin E2 regulates Th17 cell differentiation and function through cyclic AMP and EP2/EP4 receptor signaling. *J Exp Med.* 2009;206(3):535-48.
37. Maseda D, et al. mPGES1-Dependent Prostaglandin E2 (PGE2) Controls Antigen-Specific Th17 and Th1 Responses by Regulating T Autocrine and Paracrine PGE2 Production. *J Immunol.* 2018;200(2):725-36.
38. Gagliani N, et al. Th17 cells transdifferentiate into regulatory T cells during resolution of inflammation. *Nature.* 2015;523(7559):221-5.
39. Nagaya T, et al. Lipid mediators foster the differentiation of T follicular helper cells. *Immunol Lett.* 2017;181:51-7.

40. Gonnermann D, et al. Resistance of cyclooxygenase-2 expressing pancreatic ductal adenocarcinoma cells against gammadelta T cell cytotoxicity. *Oncoimmunology.* 2015;4(3):e988460.
41. Fenton TM, et al. Immune Profiling of Human Gut-Associated Lymphoid Tissue Identifies a Role for Isolated Lymphoid Follicles in Priming of Region-Specific Immunity. *Immunity.* 2020;52(3):557-70 e6.
42. Guinney J, et al. The consensus molecular subtypes of colorectal cancer. *Nat Med.* 2015;21(11):1350-6.
43. Lenz HJ, et al. Impact of Consensus Molecular Subtype on Survival in Patients With Metastatic Colorectal Cancer: Results From CALGB/SWOG 80405 (Alliance). *J Clin Oncol.* 2019;37(22):1876-85.
44. Venook AP, et al. Effect of First-Line Chemotherapy Combined With Cetuximab or Bevacizumab on Overall Survival in Patients With KRAS Wild-Type Advanced or Metastatic Colorectal Cancer: A Randomized Clinical Trial. *JAMA.* 2017;317(23):2392-401.
45. Hu H, et al. Perspectives on current tumor-node-metastasis (TNM) staging of cancers of the colon and rectum. *Semin Oncol.* 2011;38(4):500-10.
46. Lee YH, et al. Inhibition of the B7-H3 immune checkpoint limits tumor growth by enhancing cytotoxic lymphocyte function. *Cell Res.* 2017;27(8):1034-45.
47. Tang Z, et al. GEPIA2: an enhanced web server for large-scale expression profiling and interactive analysis. *Nucleic Acids Res.* 2019;47(W1):W556-W60.
48. Miao YR, et al. ImmuCellAI: A Unique Method for Comprehensive T-Cell Subsets Abundance Prediction and its Application in Cancer Immunotherapy. *Adv Sci (Weinh).* 2020;7(7):1902880.
49. Schmittgen TD, Livak KJ. Analyzing real-time PCR data by the comparative C(T) method. *Nat Protoc.* 2008;3(6):1101-8.

Figure 1

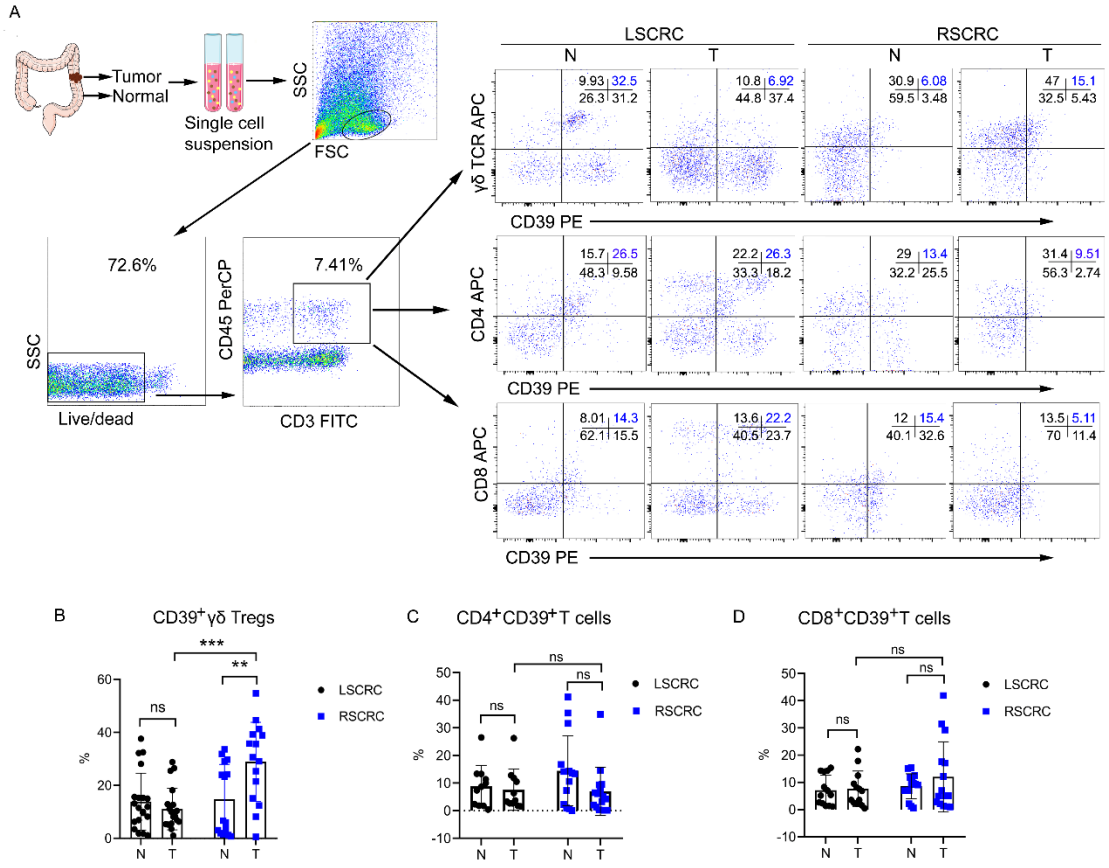

Figure 1. The infiltration of CD39$^+$γδ Tregs was significantly increased in RSCRC compared with LSCRC. (**A**) Representative flow cytometric analysis of the distribution of CD39$^+$ Tregs in CRC and paired normal tissues. The percentages of CD39$^+$ γδ Tregs (**B**), CD4$^+$ T cells (**C**) and CD8$^+$ T cells (**D**) in the total tumor-infiltrating CD3$^+$ T cells was calculated. Data are shown as mean ± SEM, two-way ANOVA followed by Sidak's multiple comparisons test; RSCRC, n=15; LSCRC, n=20; each dot represents 1 patient. N: normal; T: tumor. RSCRC, right-sided colorectal cancer; LSCRC, left-sided colorectal cancer. $^{**}P < 0.01$, $^{***}P < 0.001$, ns, no significant difference.

Figure 2

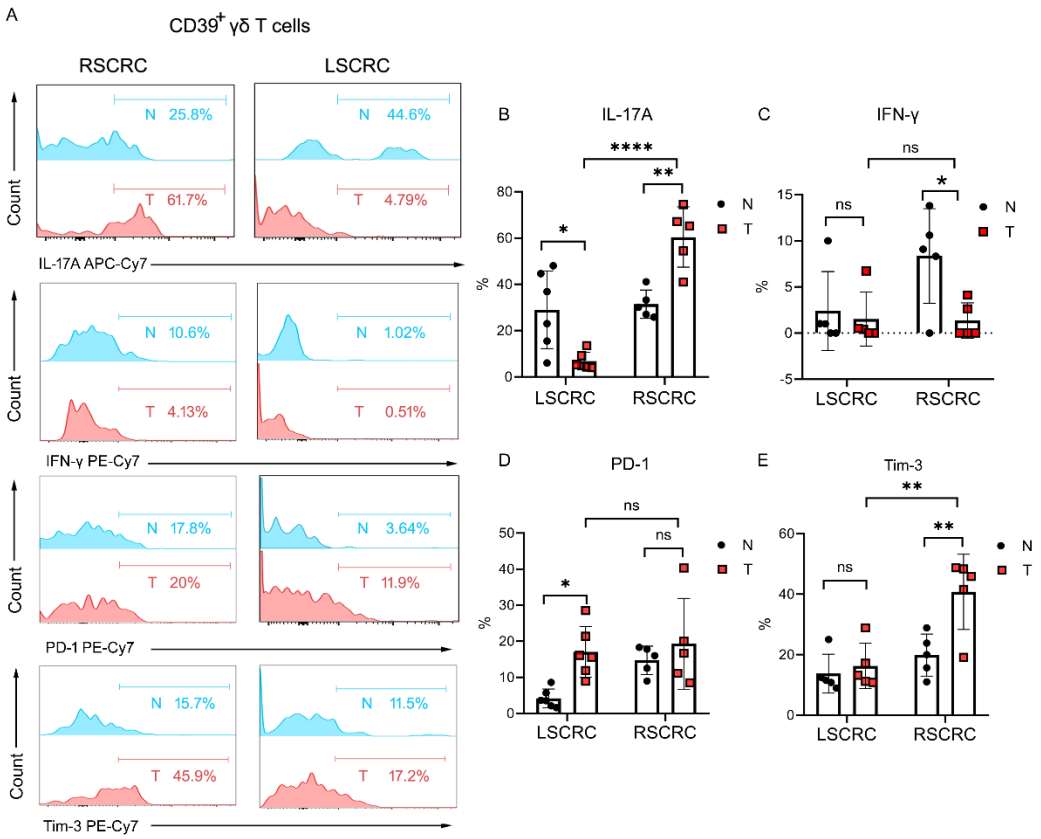

Figure 2. Differentiation phenotype of CD39$^+$γδ Tregs in RSCRC/LSCRC. (**A**) Representative histogram plot of the expression of IL-17A/IFN-γ/PD-1/Tim-3 in/on CD39$^+$ Tregs derived from LSCRC/RSCRC. The percentages of IL-17A (**B**), IFN-γ (**C**), PD-1 (**D**) and Tim-3 (**E**) in CD39$^+$γδ T cells was calculated. Data are shown as mean ± SEM, two-way ANOVA followed by Sidak's multiple comparisons test; RSCRC, n=5; LSCRC, n=6, each dot represents 1 patient. N: normal; T: tumor. RSCRC, right-sided colorectal cancer; LSCRC, left-sided colorectal cancer. *P < 0.05, **P < 0.01, ****P < 0.0001.

Figure 3

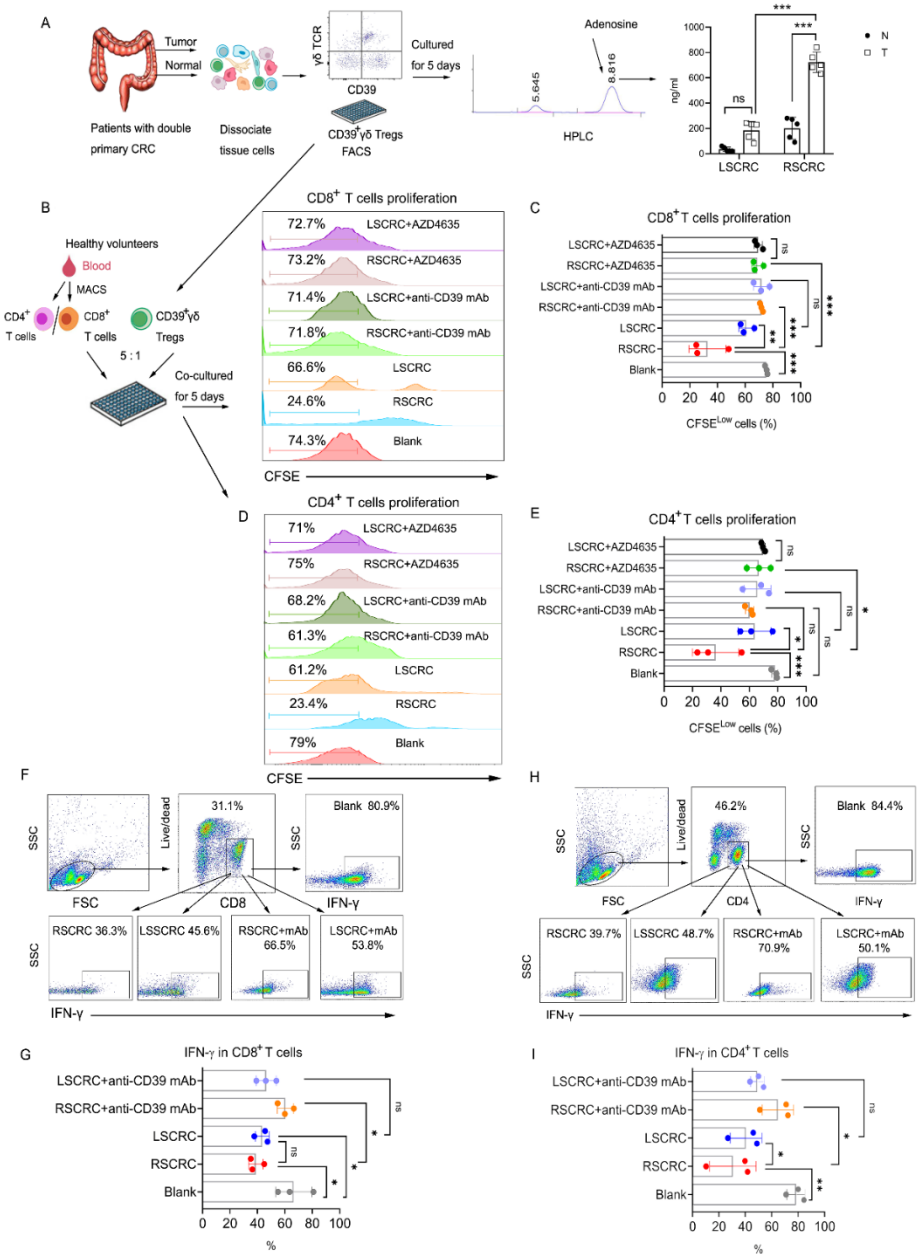

Figure 3. CD39$^+$γδ Tregs derived from RSCRC showed enhanced immunoregulatory function compared to LSCRC. (**A**) HPLC assay to measure adenosine concentrations in the supernatants of CD39$^+$γδ Tregs on day 5. Data are shown as mean ± SEM, two-way ANOVA followed by Sidak's multiple comparisons test; n=5/group. (**B-E**) Sorted CD39$^+$γδ Tregs from RSCRC and LSCRC were in vitro co-cultured with CFSE-labeled allogeneic CD4$^+$/CD8$^+$ T cells in the presence of CD3 and CD28 mAbs. Representative histogram plot of CD8$^+$ T cells (**B**) and CD4$^+$ T cells (**D**) were shown. Bar diagram summarizes the percentages of proliferated cells (CFSE^{low}) in CD8$^+$ T cells (**C**) and CD4$^+$ T cells (**E**). (**F-I**) Representative flow cytometric analysis of IFN-γ in CD8$^+$ T cells (**F**) and CD4$^+$ T cells (**H**). The percentages of IFN-γ$^+$ cells in CD8$^+$ T cells (**G**) and CD4$^+$ T cells (**I**) was summarized. One-way ANOVA followed by Tukey's multiple comparison test was used for multiple-group analysis. Data are shown as mean ± SEM. RSCRC, n=3; LSCRC, n=3 from 3-5 independent experiments. *P < 0.05; **P < 0.01; ***P < 0.001; ns, no significant difference.

Figure 4

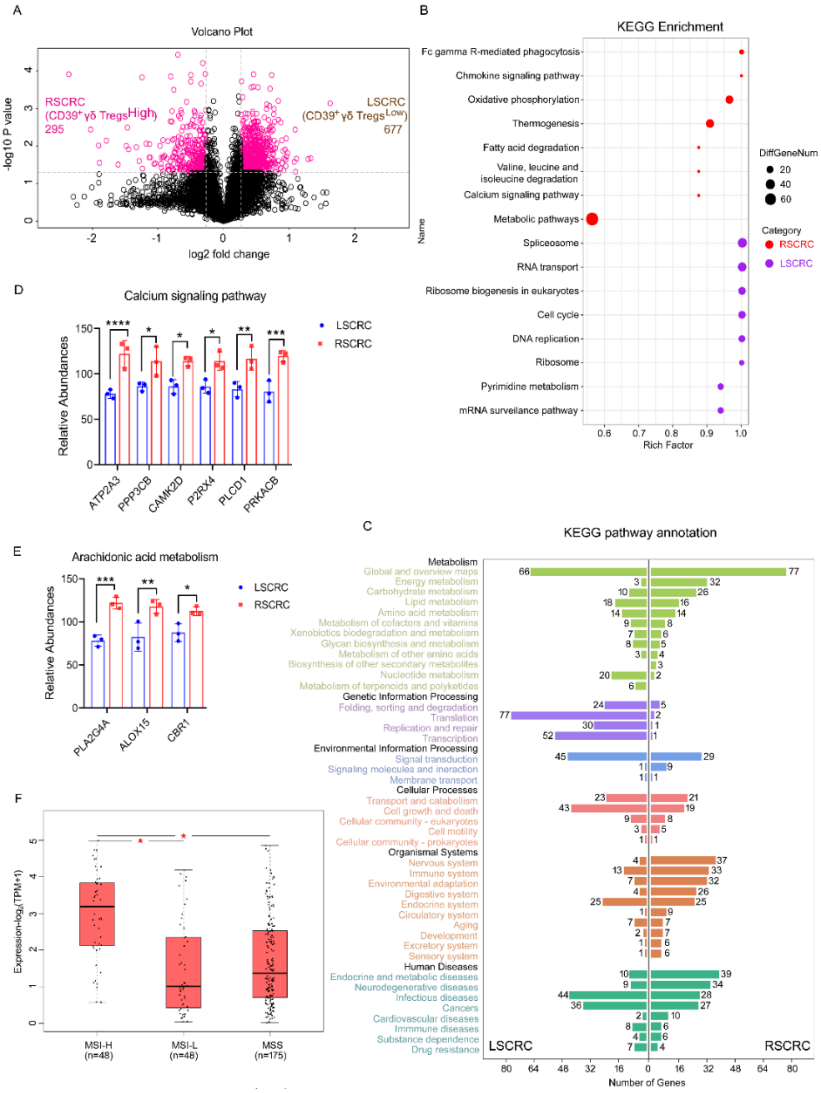

Figure 4. Difference of microenvironment between RSCRC and LSCRC. (**A**) The surgical specimens of RSCRC (n=3) with high expression of CD39^{+}γδ Tregs and the LSCRC (n=3) with low expression of CD39^{+}γδ Tregs detected by flow cytometry were then analyzed by Tandem Mass Tag (TMT)-based quantitative proteomics. The profiling experiments resulted in quantification of 972 differential proteins, among them, 295 high expression proteins were found in RSCRC and 677 in LSCRC. A volcano plot indicating results from protein-level differential analysis comparing RSCRC to LSCRC samples. Dotted lines indicated the cutoffs used to define regulated proteins (log2 FC>±1.2, adjusted *p* value<0.05). (**B**) A bubble chart displayed KEGG enrichment pathway of abnormal expression proteins in RSCRC/LSCRC. (**C**) Bar plot of secondary classification of KEGG pathway annotation highlighted features of RSCRC/LSCRC microenvironment. (**D-E**) The expression of calcium signaling pathway-related proteins (**D**) and arachidonic acid metabolism-related proteins (**E**) in RSCRC and LSCRC analyzed by quantitative proteomics. Data represent mean ± SEM. Two-way ANOVA followed by Sidak's multiple comparisons test. (**F**) *PLA2G4A* mRNA expression in colorectal cancer with MSI-High/-Low or MSS based on data obtained from the GEPIA database. One-way ANOVA test was used. MSI, microsatellite instability; MSS, microsatellite stable. *P < 0.05; **P < 0.01; ***P < 0.001; ****P < 0.0001.

Figure 5

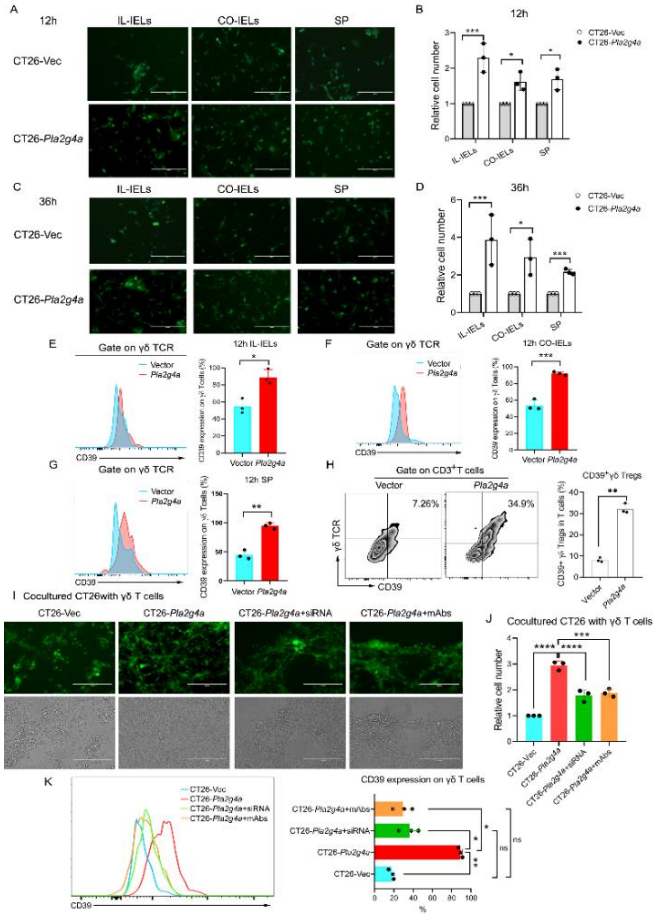

Figure 5. Overexpression of *Pla2g4a* in CT26 induced CD39$^+$γδ Tregs in vitro. (**A**) CT26-*Pla2g4a* and CT26-Vec cells were cocultured with intraepithelial lymphocytes derived from the ileum (IL-IELs), colon (CO-IELs), or spleen of BALB/c mice. Representative pictures showed the number of CT26 cells in the coculture system after 12 (**A**) and 36 hours (**C**). Scale bars: 200 μm. Bar diagram summarizes the cell numbers of CT26-*Pla2g4a* and CT26-Vec cells co-cultured with IL-IELs after 12 (**B**) and 36 (**D**) hours. Data are shown as mean ± SEM, two-way ANOVA followed by Sidak's multiple comparisons test. (**E-G**) Representative histogram plot and bar diagram summarizes the expression of CD39 on γδ T cells in IL-IELs (**E**), CO-IELs (**F**) and splenocytes (**G**) group. (**H**) Representative flow cytometric analysis of CD39$^+$Tregs in the total CD3$^+$ T cells from splenocytes. Bar diagram summarizes the percentages of CD39$^+$γδ Tregs. Unpaired *t* test was used to compare variables. (**I**) Silencing Pla2g4a in CT26-*Pla2g4a* rescued the anti-tumor response mediated by γδ T cells. CT26-*Pla2g4a* were transfected with *Pla2g4a* siRNA or control siRNA. After 24h, CT26-Vec, CT26-*Pla2g4a* and CT26-*Pla2g4a* knock down cells were co-cultured with γδ T cells sorted from BALB/c mice with or without anti-PLA2G4A antibody (5mg/ml). Bar diagram summarizes the cell number of CT26 (**J**). Representative histogram plot of CD39 expression on γδ T cells in each group by flow cytometry (**K**). Bar diagram summarizes the frequency of CD39$^+$ γδ Tregs/γδ T cells. One-way ANOVA followed by Tukey's multiple comparison test was used for multiple-group analysis. All of the experiments were repeated three times; n=3/group. **P* < 0.05, ***P* < 0.01, ****P* < 0.001, *****P* < 0.0001; ns, no significant difference.

Figure 6

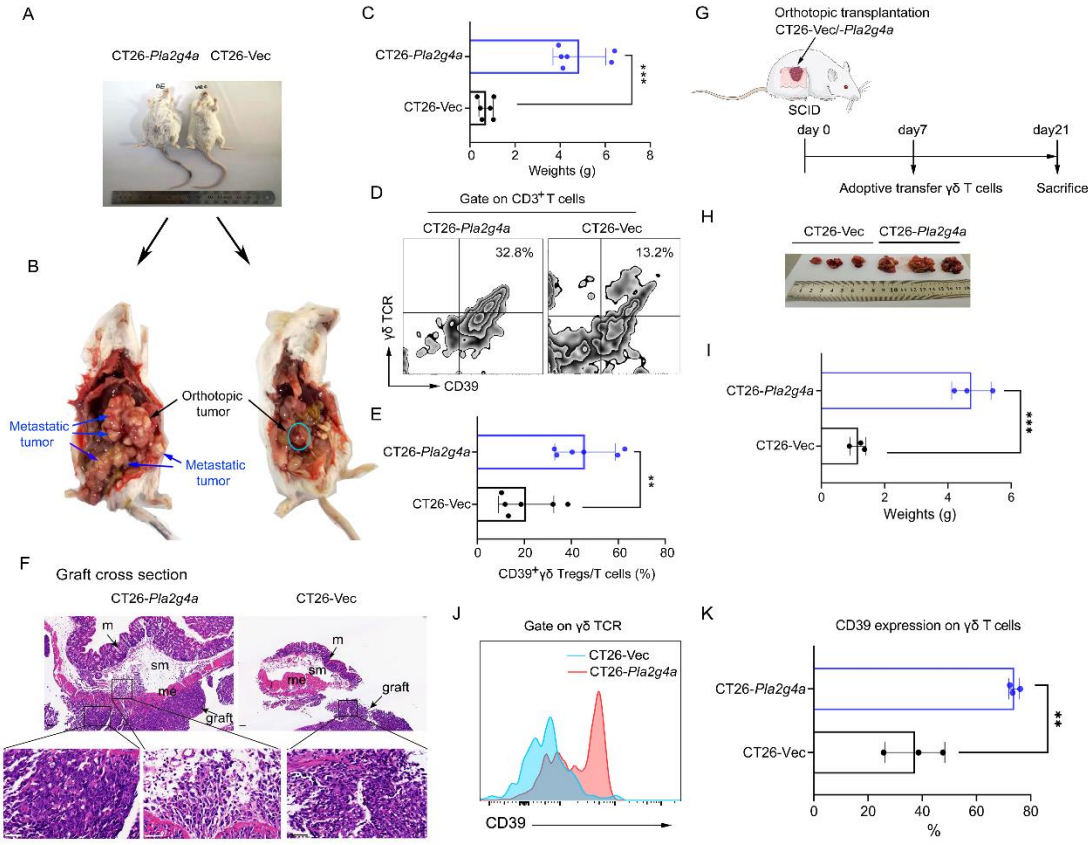

Figure 6. Overexpression of *Pla2g4a* in CT26 induced CD39^{+}γδ Tregs using orthotopic murine models of colorectal cancer. (**A**) Approximately 3-4 weeks after surgically transplanted CT26-*Pla2g4a* and CT26-Vec cells in the caecal submucosa of BALB/c mice, bloody ascites occurred, and the abdomen increased significantly in the CT26-*Pla2g4a* group. n=6 per group. (**B**) The orthotopic tumor and metastatic tumor in the colon. (**C**) The tumor weight was robustly increased in the CT26-*Pla2g4a* group. (**D**) The frequency of CD39^{+}γδ Tregs infiltrated in the orthotopic tumors in the two groups. (**E**) The weights of orthotopic tumors were calculated. (**F**) Representative H&E staining of graft cross-section in orthotopic tumor. (**G**) Schematic of SCID mice experimental design. n=3 per group. (**H**) The tumor size was shown. (**I**) Scatter diagram summarizes the weights of orthotopic tumors. (**J**) Representative histogram plot of CD39 expression on γδ T cells in each group by flow cytometry. (**K**) The scatter diagram summarizes the frequency of CD39 positive cells. M, mucosa; me, muscolaris externa; sm, submucosa. Data shown are representative of 3 independent experiments. Data are shown as mean ± SEM. Unpaired *t* test was used to compare variables. ** $P < 0.01$, ***$P < 0.001$. Scale bars, 50 μm.

Figure 7

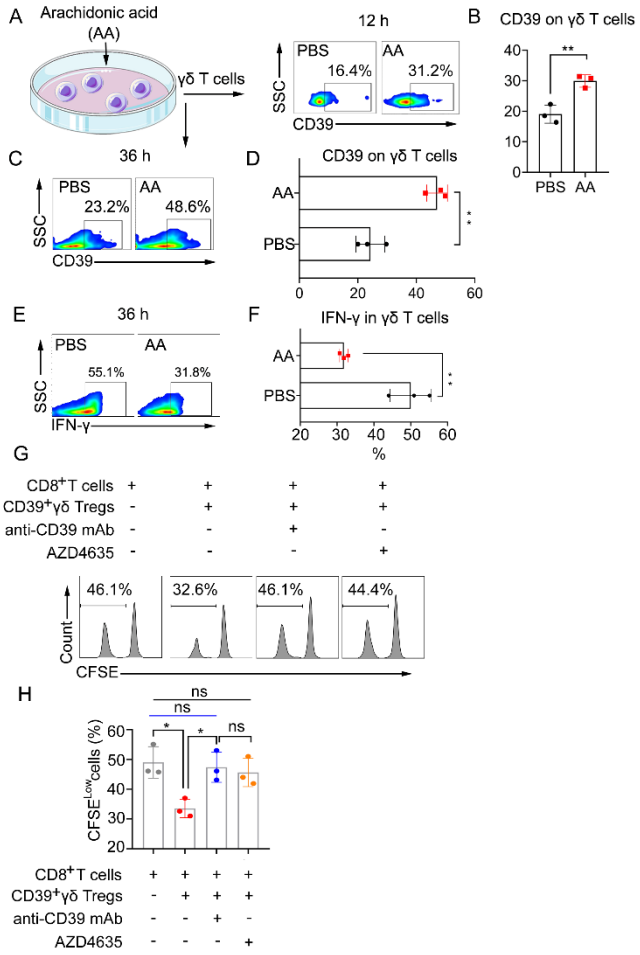

Figure 7. Exogenous AA promotes CD39$^+$γδ Tregs polarization in vitro. (**A-D**) Exogenous AA (5μM) induced the expression of CD39 on γδ T cells. γδ T cells sorted from BALB/c mice were treated with AA (5μM) in vitro, and the expression of CD39 on γδ T cells was determined by flow cytometry at 12h (**A**) and 36h (**C**). The percentages of CD39 positive cells at 12h (**B**) and 36h (**D**) were calculated and compared using an unpaired *t*-test (n = 3). (**E**) Exogenous AA (5μM) decreased the production of IFN-γ in γδ T cells. The percentages of IFN-γ positive cells by intracellular staining at 36h (**F**) were calculated and compared using an unpaired *t*-test (n = 3). (**G**) AA-induced-CD39$^+$γδ Tregs inhibited the proliferation of CD8$^+$cells. AA-induced-CD39$^+$γδ Tregs sorted by flow cytometry were then mix with CFSE-labeled αβ T cells from BALB/c mice at a 1:5 ratio and activated by anti-CD3/CD28 mAb with or without anti-CD39 mAb/A2AR inhibitor AZD4635. CFSE was determined by flow cytometry, gating on CD8$^+$cells. (**H**) Percentage of CFSE-low cells were calculated and compared using one-way ANOVA followed by Tukey's multiple comparison test (n = 3). Data are represented as mean ± SEM of 2-3 independent experiments.

Figure 8

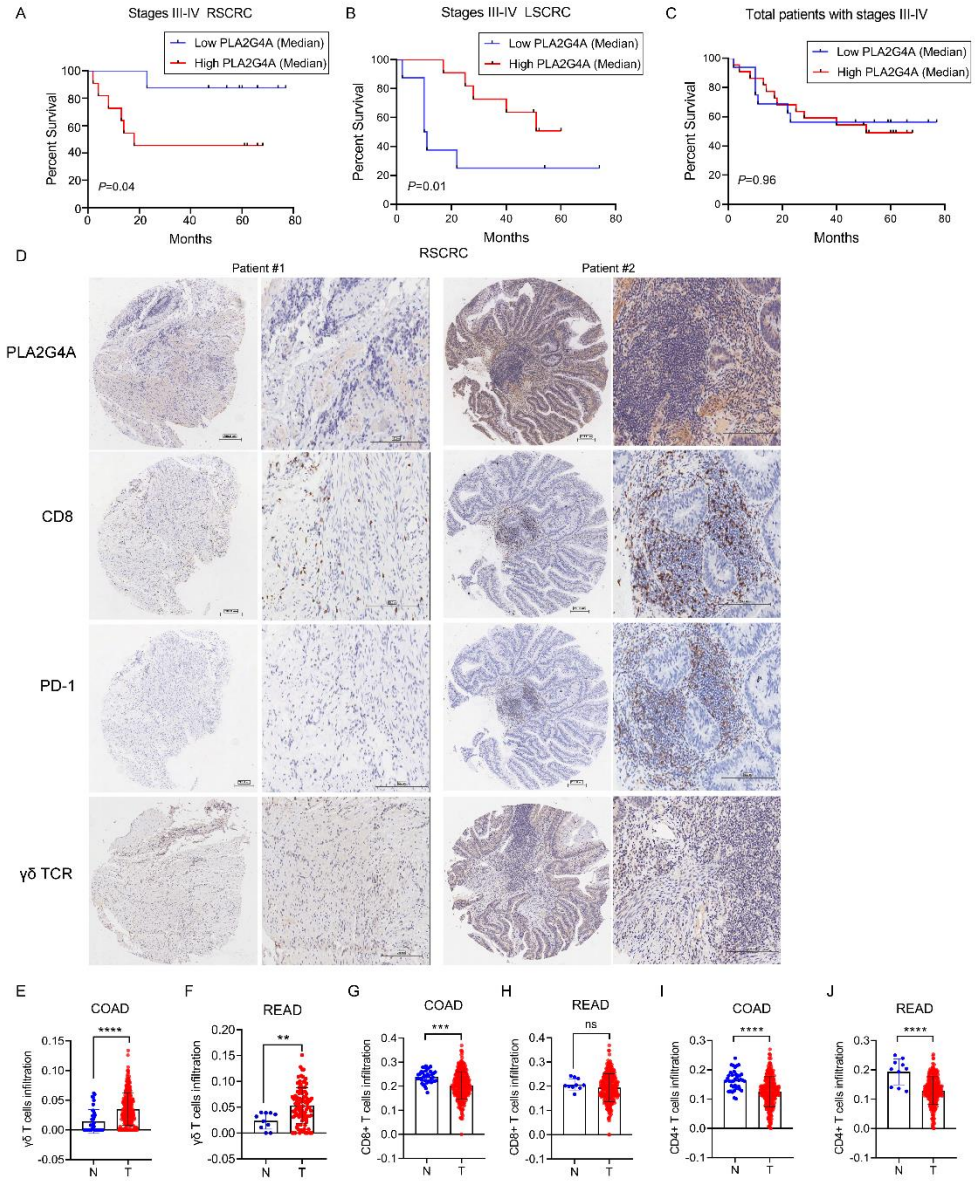

Figure 8. The relationship between PLA2G4A expression and the prognosis of patients with colorectal cancer. (**A**) Kaplan-Meier overall survival curves showed high-level expression of PLA2G4A correlated with poor prognosis in stage III-IV RSCRC. n=20. (**B**) III-IV stage LSCRC patients with high-level of PLA2G4A had a better outcome in overall survival. n=18. (**C**) Kaplan-Meier overall survival curves of CRC patients. Log-rank test were used for analysis. n=38. PLA2G4A median level was used as cutoff. (**D**) The representative IHC staining of PLA2G4A, CD8, PD-1 and γδ TCR expression in RSCRC samples (Patient 1 survival: 77 months, alive; Patient 2 survival: 14 months, dead). (**E-F**) The infiltration of γδ T cells in COAD (**E**) and READ (**F**). (**G-H**) The infiltration of $CD8^+$ T cells in COAD (**G**) and READ (**H**). (**I-J**) The infiltration of $CD4^+$ T cells in COAD (**I**) and READ (**J**). COAD, n=288, Normal, n=40; READ, n=95, Normal, n=10. COAD, colon adenocarcinoma; READ, rectum adenocarcinoma. Data are shown as mean ± SEM. Unpaired *t* test was used to compare variables. ** $P < 0.01$, ***$P < 0.001$, ****$P < 0.0001$, ns, no significant difference.

Table 1. Correlation between $CD39^+$ γδ T cells expression and clinicopathological parameters of colorectal cancer.

	Frequency of $CD39^+$ γδ Tregs (%)			
Characteristics	Total (cases)		*P* value	Spearman correlation coefficient
Total	35	18.70±14.35		
Age (years)			0.871	0.029
＜65	20	17.71±12.45		
≥65	15	20.03±16.92		
Gender			0.268	0.192
Male	17	21.23±15.77		0.192
Female	18	16.31±12.86		
Tumor size (cm)			0.722	0.062
＜5	18	17.82±15.50		
≥5	17	19.64±13.47		
Tumor site			0.001**	0.595
Right	15	28.87±14.94		
Left	20	11.08±7.83		
Tumor stage			0.001**	0.522
I-II	16	11.68±11.90		
III-IV	19	24.62±13.79		
Lymphatic metastasis			0.001**	0.522
Yes	19	24.62±13.79		
No	16	11.68±11.90		

Correlation between variables were assessed by Spearman rank correlation test. Data represent mean ± standard deviation. $^{**}P < 0.01$

Table 2 Clinicopathological characteristics of patients with different PLA2G4A expression levels undergoing surgery for stage III-IV colorectal cancer.

		Expression of PLA2G4A (cases)		
Characteristics	Total (cases)	Low	High	*P* value
Total	20	10 (50%)	10 (50%)	
Age (years)				
＜65	7	2 (28.6%)	5 (71.4%)	0.160
≥65	13	8 (61.5%)	5 (38.5%)	
Gender				
Male	7	2 (28.6%)	5 (71.4%)	0.160
Female	13	8 (61.5%)	5 (38.5%)	
Tumor size (cm)				0.160
＜5	7	2 (28.6%)	5 (71.4%)	
≥5	13	8 (61.5%)	5 (38.5%)	
Perineuralinvasion				0.329
-	14	8 (57.1%)	6 (42.9%)	
+	6	2 (33.3%)	4 (66.6%)	
Vascularinvasion				0.178
-	11	7 (63.6%)	4 (36.4%)	
+	9	3 (33.3%)	6 (66.7%)	
γδ TCR expression				0.010*
Low	11	9 (81.8%)	2 (18.2%)	
High	9	1 (11.1%)	8 (88.9%)	
CD8 expression				0.025*
-	9	7 (77.8%)	2 (22.2%)	
+	11	3 (27.2%)	8 (72.7%)	
PD-1 expression				0.010*
-	15	10 (66.7%)	5 (33.3%)	
+	5	0 (0%)	5 (100%)	
PD-L1 expression				0.686
-	14	7 (50%)	7 (50%)	
+	6	3 (50%)	3 (50%)	

Differences between experimental groups were assessed by Likelihood ratio χ^2 test. *$P < 0.05$; **$P < 0.01$. PLA2G4A or γδ TCR median level was used as cutoff.

Table 3 Clinicopathological characteristics of patients with different PLA2G4A expression levels undergoing surgery for stage I-IV RSCRC.

		Expression of PLA2G4A (cases)		
Characteristics	Total (cases)	Low	High	*P* value
Total	46	10 (50%)	10 (50%)	
Age (years)				
＜65	18	4 (22.2%)	14 (77.8%)	0.097
≥65	13	13 (46.4%)	15 (53.6%)	
Gender				
Male	7	2 (28.6%)	5 (71.4%)	0.160
Female	13	8 (61.5%)	5 (38.5%)	
Tumor size (cm)				0.315
＜5	15	4 (26.7%)	11 (73.3%)	
≥5	31	13 (41.9%)	18 (58.1%)	
Lymph node metastasis				0.108
-	26	7 (26.9%)	19 (73,1%)	
+	20	10 (50%)	10 (50%)	
Perineuralinvasion				0.329
-	40	15 (37.5%)	25 (62.5%)	
+	6	2 (33.3%)	4 (66.6%)	
Vascularinvasion				0.956
-	30	11(36.7%)	19(63.3%)	
+	16	6 (37.5%)	10 (62.5%)	
CD8 expression				0.828
-	28	10 (35.7%)	18 (64.3%)	
+	18	7 (38.9%)	11 (61.1%)	
PD-1 expression				0.017*
-	34	16 (47.1%)	18 (52.9%)	
+	12	1 (8.3%)	11(91.7%)	
PD-L1 expression				0.276
-	34	11 (32.4%)	23 (67.6%)	
+	12	6 (50%)	6(50%)	

Differences between experimental groups were assessed by Pearson χ^2 test. *$P < 0.05$. PLA2G4A median level was used as cutoff.